Tumorigenicity of hypoxic respiring cancer cells revealed by a hypoxia–cell cycle dual reporter

Anne Le[a,b,1,2], Zachary E. Stine[c,1], Christopher Nguyen[a], Junaid Afzal[d], Peng Sun[d], Max Hamaker[a], Nicholas M. Siegel[a], Arvin M. Gouw[b], Byung-hak Kang[b], Shu-Han Yu[b], Rory L. Cochran[e], Kurt A. Sailor[f], Hongjun Song[f], and Chi V. Dang[a,b,c,d,e,2]

[a]Department of Pathology and Oncology, [b]Graduate Program in Pathobiology, [d]Department of Medicine, [e]Graduate Program in Cellular and Molecular Medicine, and [f]Stem Cell Program, Institute for Cell Engineering, Department of Neurology, The Johns Hopkins University School of Medicine, Baltimore, MD 21231; and [c]Abramson Family Cancer Research Institute, Abramson Cancer Center of the University of Pennsylvania, Philadelphia, PA 19104

Edited by Ronald A. DePinho, University of Texas MD Anderson Cancer Center, Houston, TX, and approved July 14, 2014 (received for review February 3, 2014)

Although aerobic glycolysis provides an advantage in the hypoxic tumor microenvironment, some cancer cells can also respire via oxidative phosphorylation. These respiring ("non-Warburg") cells were previously thought not to play a key role in tumorigenesis and thus fell from favor in the literature. We sought to determine whether subpopulations of hypoxic cancer cells have different metabolic phenotypes and gene-expression profiles that could influence tumorigenicity and therapeutic response, and we therefore developed a dual fluorescent protein reporter, HypoxCR, that detects hypoxic [hypoxia-inducible factor (HIF) active] and/or cycling cells. Using HEK293T cells as a model, we identified four distinct hypoxic cell populations by flow cytometry. The non-HIF/noncycling cell population expressed a unique set of genes involved in mitochondrial function. Relative to the other subpopulations, these hypoxic "non-Warburg" cells had highest oxygen consumption rates and mitochondrial capacity consistent with increased mitochondrial respiration. We found that these respiring cells were unexpectedly tumorigenic, suggesting that continued respiration under limiting oxygen conditions may be required for tumorigenicity.

antiangiogenesis | metabolism | mitochondria

Changes in cancer-cell metabolism have been linked to genetic alterations of oncogenes, tumor suppressors, and metabolic enzymes (1–3). The hypoxic tumor microenvironment further modifies metabolism through activation of hypoxia-inducible factors (HIFs). The HIFs enhance tumorigenesis by stimulating glycolysis, cell motility, and angiogenesis (4, 5). Thus, hypoxia portends poor prognosis in common cancers, such as gastric, lung, ovarian, pancreatic, prostate, and renal carcinomas (5).

Although Otto Warburg observed respiration in certain cancer types, his obsession with aerobic glycolysis as a cause of cancer promulgated the prevailing misconception that cancers only exhibit the Warburg effect exclusive of respiration (6). Because the hypoxic tumor microenvironment activates HIFs and diminishes respiration, whether hypoxia enhances tumorigenicity at the expense of respiration is not fully understood (7). We found recently that oxidative and glycolytic metabolism coexist in hypoxic B lymphocytes, such that the shunting of glucose to lactate away from the tricarboxylic acid cycle (TCA) cycle by hypoxia is compensated through glutamine oxidation in the TCA cycle (8). These metabolic aberrations suggest the existence of hypoxic respiring (herein termed non-Warburg) cells capable of continued oxidative metabolism under hypoxic conditions. Further, it is believed that cancer cells within the tumor microenvironment are either aerobic or hypoxic because of oxygen gradients coming from nearby imperfect blood vessels. An intriguing commensal metabolic relationship between hypoxic and aerobic cells has been documented, whereby hypoxic cells produce lactate that is converted to pyruvate for respiration by aerobic cancer cells located nearby the blood vessel (9). We hypothesize, however, that hypoxic respiring cells could also participate in this commensal relationship, specifically because oxygen becomes limiting for cytochrome *c* oxidase and cellular respiration only around 0.1% and 0.5% oxygen, respectively (10). In this regard, we sought to determine the gene expression and tumorigenic phenotypes of these putative non-Warburg cells and other hypoxic tumor-cell subpopulations. Toward this end, we developed a reporter system that identifies hypoxic and/or cycling cells.

We constructed a dual fluorescent protein reporter system—hypoxia and cell cycle reporter (HypoxCR)—that simultaneously detects hypoxic and/or dividing cells. Using HEK293T cells stably expressing HypoxCR as a model, we identified and purified four distinct hypoxic cell populations by flow cytometry. We surmise that these four populations reflect the heterogeneity of the solid tumor microenvironment that we observed by microscopy in HEK293T xenografts. Each hypoxic cell subpopulation has distinct gene-expression profiles. The population that was HIF-negative and noncycling had increased expression of mitochondrial genes. As a purified population, these non-HIF/noncycling cells also had the highest oxygen-consumption rate and mitochondrial capacity. Surprisingly, we found that these cells were tumorigenic in xenografts, similar to the cells that were HIF-positive and cycling. Neither HIF-positive noncycling cells nor cycling HIF-negative cells were capable of establishing tumor xenografts. Furthermore, we provide proof-of-concept studies for the use of HypoxCR in vivo and found that bevacizumab (VEGF pathway inhibitor) increased the HIF-positive cell population, consistent with a vascular pruning effect.

Results and Discussion

HypoxCR, a Dual Fluorescent Protein Reporter, Identifies Subpopulations of Hypoxic HEK293T Cells. We sought to understand whether subpopulations of hypoxic cancer cells have different gene-expression

Significance

In this study, we report the finding that a subpopulation of hypoxic cancer cells expressed genes involved in mitochondrial function, sustained oxidative metabolism, and were fully tumorigenic. These findings indicate that, whereas the Warburg effect contributes to the metabolism of growing cancer cells, tumorigenicity does not exclusively depend on it and is not diminished by continued respiration under hypoxia.

Author contributions: A.L. and C.V.D. designed research; A.L., Z.E.S., C.N., J.A., P.S., M.H., N.M.S., A.M.G., B.-h.K., S.-H.Y., R.L.C., K.A.S., and H.S. performed research; A.L., Z.E.S., C.N., J.A., P.S., and C.V.D. analyzed data; and A.L., Z.E.S., and C.V.D. wrote the paper.

Conflict of interest statement: C.V.D. has an equity interest in Agios Pharmaceuticals, Inc.

This article is a PNAS Direct Submission.

Freely available online through the PNAS open access option.

[1]A.L. and Z.E.S. contributed equally to this work.

[2]To whom correspondence may be addressed. Email: dangvchi@exchange.upenn.edu or annele@jhmi.edu.

This article contains supporting information online at www.pnas.org/lookup/suppl/doi:10.1073/pnas.1402012111/-/DCSupplemental.

profiles and metabolic phenotypes that might influence tumorigenicity and therapeutic responses. Toward this end, we developed a dual fluorescent protein reporter, HypoxCR, that detects hypoxic and/or cycling cells (Fig. 1*A*). We initially characterized a series of vectors with five hypoxia responsive elements (HREs) driving expression of GFP fusion proteins and found that a sequence enriched for proline, glutamate, serine, and threonin (PEST) degron is sufficient to confer the desired shortened half-life of GFP that is essential to detect HIF activity in real-time and its changes with reoxygenation, which is commonly found in the tumor microenvironment (11–13) (Fig. S1 and *SI Text*). Based on these studies, we found that two HREs were sufficient for the hypoxic response of the short-lived GFP and used this cassette to build HypoxCR (Fig. 1*B* and Fig. S1). HypoxCR consists of two expression cassettes: a PEST destabilized GFP cDNA driven by two *VEGFA* hypoxia responsive elements (HREs) and a pCMV-driven fusion gene producing mCherry-geminin, which is stabilized in S-G_2M phases of the cell cycle (Fig. S1*C*) (14). The two expression cassettes are separated by a spacer sequence (see *SI Text* for full vector construction and validation).

We generated a stable HEK293T cell line that expresses HypoxCR (293T-HypoxCR cells), purified it (Fig. S2 *A*–*C*), and then characterized it by flow cytometry (Fig. 1 *C*–*F*). Under aerobic conditions, the 293T-HypoxCR cells displayed two major populations of $GFP^-/mCherry^-$ (termed non-HIF/noncycling or non-Warburg) and $GFP^-/mCherry^+$ (termed non-HIF/cycling) cells (Fig. 1*D*). Upon exposing the 293T-HypoxCR cells to 16 h of 2% oxygen (hypoxia), two additional HIF-positive populations became apparent: $GFP^+/mCherry^-$ (termed HIF/noncycling) and $GFP^+/mCherry^+$ (termed HIF/cycling) cells (Fig. 1*E*).

We then mimicked the dynamic changes of blood flow in tumors, which caused cycles of oxygen deprivation and subsequent reoxygenation, by exposing cells to 2% oxygen for 16 h and then returning them to 21% oxygen for an extra 4 h (13). We observed an increase in mCherry-positive cells: the non-HIF/cycling and HIF/cycling subpopulations, which we speculate may have arisen from the non-HIF/noncycling and HIF/noncycling cells, respectively (Fig. 1*F*). This observation is consistent with our previous identification of a hypoxia-induced G1 checkpoint and the ability of HIF-1α to inhibit DNA replication (15–17). We speculate that reoxygenation relieved this checkpoint, permitting the entry of noncycling cells into S-G_2M phases of the cell cycle as observed in Fig. 1*F*. We then used this condition in vitro to model the heterogeneity of hypoxic tumor cells in vivo.

To ensure that the HRE-driven GFP reflects HIF-1α activity, we overexpressed a stabilized HIF-1α with mutations at three proline residues, which render the HIF-1α mutant resistance to prolyl hydroxylation and subsequent proteasomal degradation (18), and

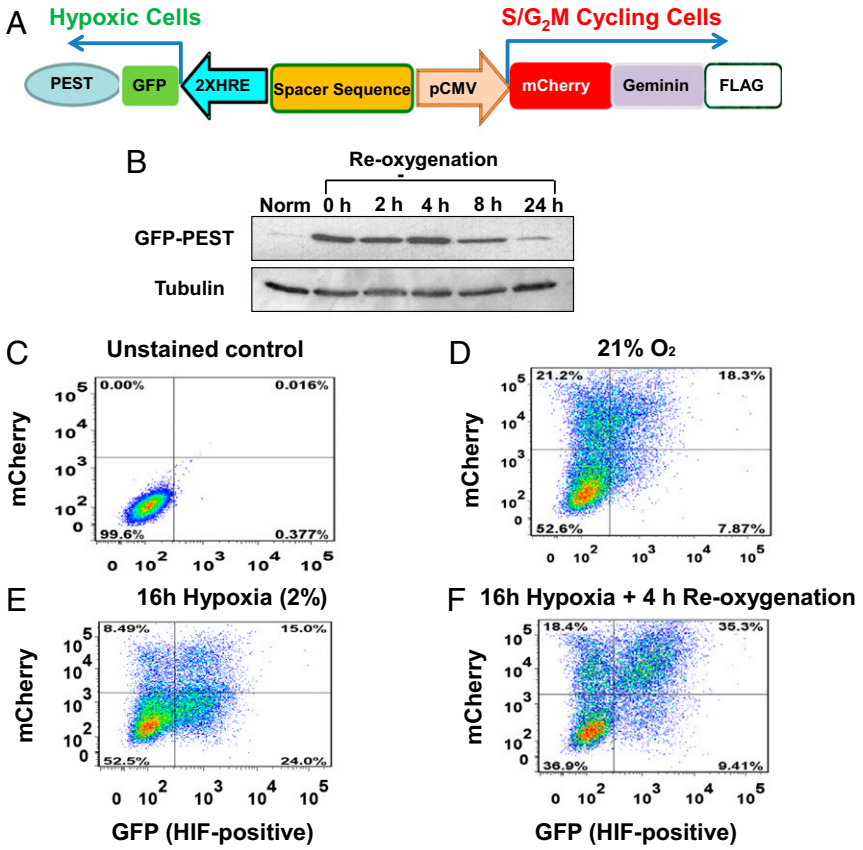

Fig. 1. (*A*) Schema of the HypoxCR dual fluorescent reporter of hypoxia and cell cycling. HypoxCR consists of two expression cassettes flanking a spacer sequence. The hypoxia responsive cassette is shown with two hypoxia response element (2xHRE) driving the expression of a fusion gene of green fluorescent protein (GFP) and a PEST degron. The cell-cycling reporter cassette consists of a CMV promoter driving expression of a fusion of mCherry and geminin tagged with FLAG. Arrows depict transcriptional start sites. (*B*) HRE-driven short-lived GFP as a hypoxia reporter. Immunoblots of GFP at various times (in hours) of reoxygenation following 16 h of hypoxia (2% oxygen). Norm, lysates from cells unexposed to hypoxia. Flow-cytometric analysis of control and 293T-HypoxCR cells. (*C*) Analysis of control cells without HypoxCR, gating on mCherry and GFP fluorescence. (*D*) 293T-HypoxCR cells analyzed upon culturing in 21% oxygen. (*E*) 293T-HypoxCR cells exposed to 16 h of 2% oxygen. (*F*) 293T-HypoxCR cells exposed to 16 h of hypoxia followed by 4 h of reoxygenation. 293T-HypoxCR cells were grown in tissue culture for less than 3 wk, and this experiment was performed before all other experiments to ensure the dynamics of these subpopulations.

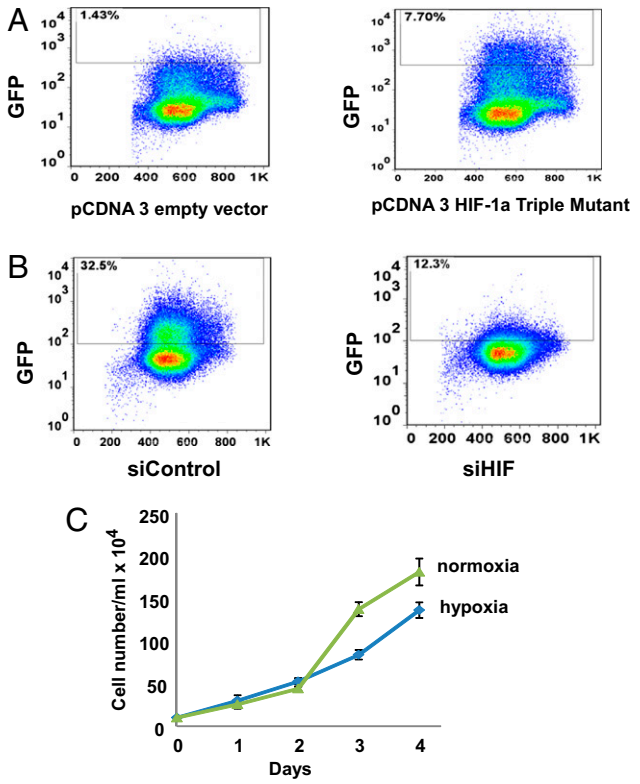

Fig. 2. (*A*) Transient expression of a stabilized mutant HIF-1α–induced HRE-driven GFP expression in normoxic cells. 293T-HypoxCR cells were transiently transfected with a stabilized mutant HIF-1α possessing mutations at three proline residues and analyzed by flow cytometry. (*B*) siRNA-mediated knockdown of HIF-1α–reduced HRE-driven GFP expression in hypoxic cells. 293T-HypoxCR cells were transiently transfected with siRNAs targeting HIF-1α, cultured in hypoxia, and then analyzed by flow cytometry. (*C*) 293T-HypoxCR cell growth under aerobic (21% oxygen) and hypoxic (2% oxygen) conditions. All cells were grown at 1×10^5 cells per mL. Cell counts were performed in triplicate and shown as mean ± SD.

found an increase in GFP-positive aerobic 293T-HypoxCR cells (Fig. 2*A*). Conversely, we document that loss of HIF-1α through siRNA-mediated inhibition of expression resulted in a markedly blunted GFP response under hypoxia (Fig. 2*B*).

Differential Gene Expression in Subpopulations of Hypoxic Cells Reveals a Group with Persistent Expression of Mitochondrial Genes. We sought to determine altered gene expression among the subpopulations of hypoxic 293T-HypoxCR cells to gain insight into hypoxic tumor-cell heterogeneity. 293T-HypoxCR cells are capable of proliferating under hypoxic conditions (Fig. 2*C*), making them a suitable model to study the different subpopulation of cells in hypoxia. In triplicate experiments, we flow-sorted cells similarly treated as those shown in Fig. S2*C* and performed gene-expression microarray analysis of four subpopulations of 293T-HypoxCR cells. We identified 663 differentially expressed genes with *P* values <0.03 and performed an unsupervised clustering analysis (Fig. 3) that revealed distinct expression profiles in each of the four different subpopulations (19).

The non-HIF/cycling cells appeared unique in that HIF was inactive with an associated increase in expression of genes involved in apoptosis and DNA repair as determined by gene set enrichment analysis (20) (Fig. 3, box 1). This observation implies that a subpopulation of hypoxic cells could remain in or enter into S-G_2M phases when HIF was inactive. Moreover, the HIF/cycling cells share expression of genes in common with the non-HIF/cycling cells (Fig. 3, boxes 1 and 2). Some of these genes are involved in cell cycling as well as the stress-response genes, suggesting that hypoxic cycling cells have DNA replication stress (Fig. 3, box 2). We then examined the level of phosphorylated histone H2AX (γH2AX), which signals DNA damage, and found that the double-positive and the non-HIF/cycling cells had high levels of γH2AX, suggesting that they had DNA replication stress (Fig. 4*A*).

A significant fraction of the HIF/cycling cells appear to have arisen from the HIF/noncycling cells (Fig. 1 *E* and *F*) and thus share some genes in common, such as hypoxia responsive genes (Fig. 3, box 4). Intriguingly, the GFP-positive HIF/noncycling cells have increased expression of hypoxia-inducible genes and those that are altered by polycomb proteins (Fig. 3, box 4 and Table S1). Unexpectedly, we found that the double-negative, non-HIF/noncycling cells expressed a distinct set of genes that is not seen in the other subpopulations (Fig. 3, box 3). This set is enriched with nuclear encoded mitochondrial genes as determined by gene-set enrichment analysis (20), suggesting that this subpopulation respires under hypoxia.

Non-Warburg Cells Are Tumorigenic. To characterize the metabolic states of the different hypoxic cell populations, we purified the four populations of cells by flow sorting and immediately studied

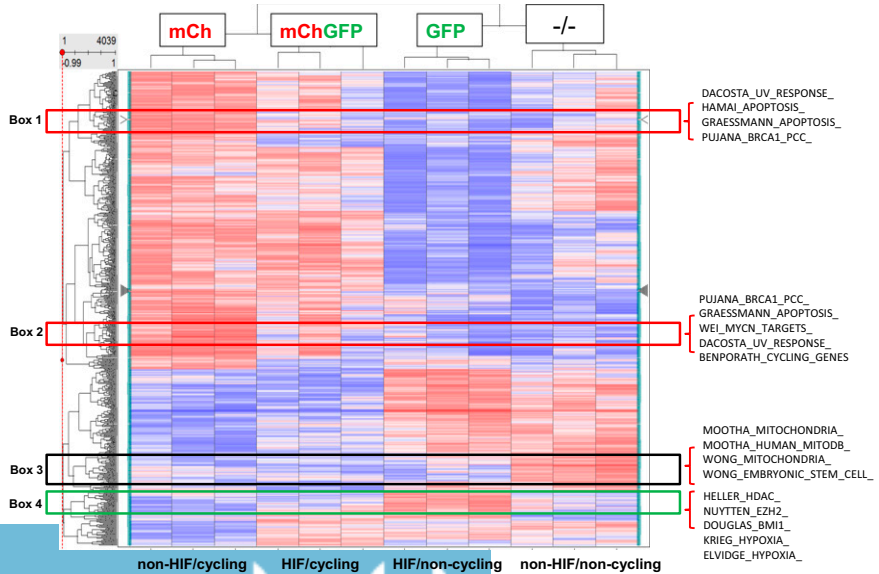

Fig. 3. Gene-expression analysis of four hypoxic subpopulations of HypoxCR-293T cells reveals distinct transcriptional profiles. Gene-expression profiles from microarray analysis of triplicate biological experiments were subjected to unsupervised clustering. Triplicate samples clustered together for each subpopulation, whose similarity to one another is shown by the dendrogram on top. The dendrogram on the left highlights genes that have similar expression profiles across the four populations with boxes 1–4 highlighting distinct features of the different populations. Gene-set enrichment analysis (GSEA) reveals features of boxed genes. Biological themes of the boxed genes are shown on the far right from the top 50 statistically significantly associated gene sets.

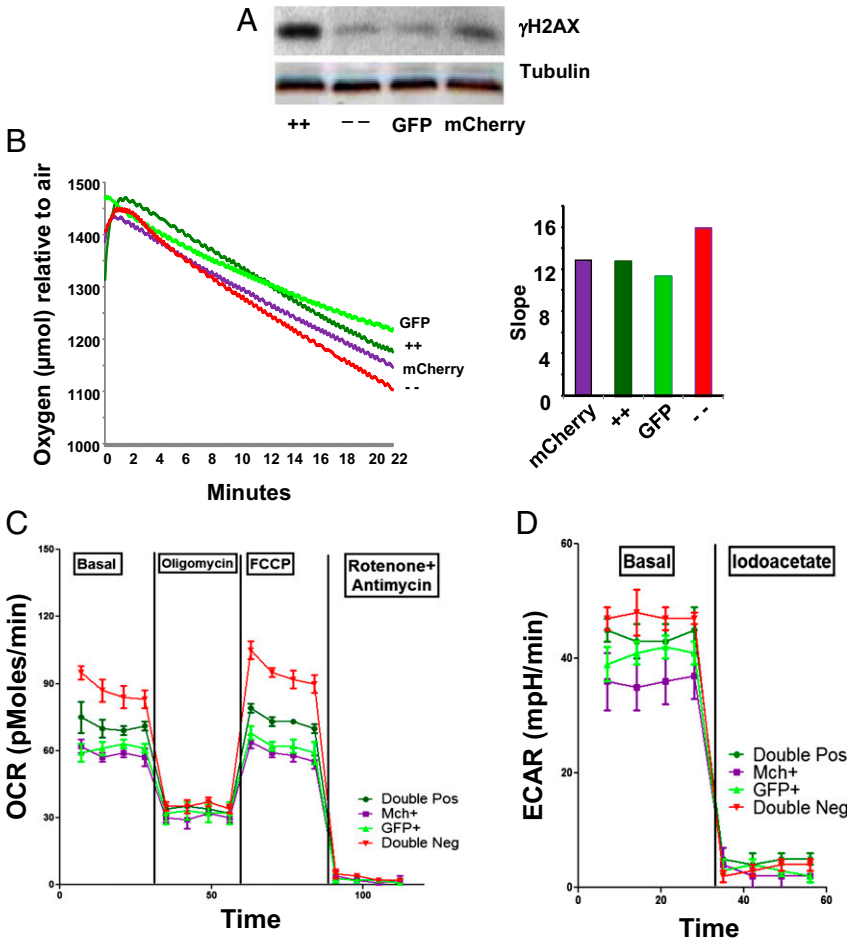

Fig. 4. (*A*) DNA breaks in subpopulations of hypoxic cells. Immunoblot of phosphorylated H2AX (γH2AX) levels in lysates from flow-sorted four subpopulations of cells cultured in hypoxia. Tubulin served as a loading control. (*B*) Oxygen consumption rates of isolated subpopulations of 293T-HypoxCR cells. Oxygen content (relative to air) in the media as a function of time was determined using a Clarke's oxygen electrode and shown color-coded as well as labeled on the far right: HIF/noncycling (GFP); HIF/cycling (+/+); non-HIF/cycling (mCherry); non-HIF/noncycling (–/–). The *Inset* represents the negative slopes of the oxygen consumption curves. (*C* and *D*) Mitochondrial respiration and glycolytic activity of each subpopulation. Cells were sorted into four subpopulations by flow cytometry, and metabolic assessments were perform by Seahorse XF^{e}96 Extracellular Flux Analyzer. (*C*) From left to right: basal mitochondrial respiration was assessed by measuring oxygen consumption rate (OCR) before adding ATP synthase inhibitor (4 μM oligomycin) or 500 nM FCCP or 300 nM Rotenone and 300 nM antimycin to inhibit electron transport chain of oxidative phosphorylation. (*D*) Basal glycolytic activity was evaluated by measuring the extracellular acidification rate (ECAR) before adding 600 μM iodoacetate to inhibit glycolysis by irreversibly inhibiting glyceraldehyde-3-phosphate dehydrogenase (GAPDH). Experiments, which were performed in biological triplicates, were repeated twice. Data were analyzed after normalization by DNA content.

them (Fig. 4*B*) (21). Using a Clarke's oxygen electrode, the non-HIF/noncycling cells were found to have the highest oxygen consumption rate, which is compatible with their gene expression profile enriched with genes involved in respiration. We further studied the cell populations using the Seahorse XFe96 Extracellular Flux Analyzer, which measures oxygen consumption rate (OCR) as an indicator of oxidative phosphorylation (OXPHOS) and extracellular acidification rate (ECAR) as an indicator of glycolytic conversion of glucose to lactate. As illustrated in Fig. 4*C*, we found that the non-HIF/noncycling cells had the highest resting OCR or OXPHOS and the highest mitochondrial capacity after treatment of cells with trifluorocarbonylcyanide phenylhydrazone (FCCP), confirming the findings using the Clarke's oxygen electrode (Fig. 4*B*). They also had the lowest ECAR to OCR ratio, suggesting that they are more oxidative than the other populations of cells. The HIF-positive cell populations, by contrast, were slightly less metabolically active and had the highest relative acidification rates (ECAR/OCR ratios: (–/–) = 0.52; (+/+) = 0.62; GFP = 0.67; mCherry = 0.61), which are consistent with increased glycolysis driven by HIF-1α (Fig. 4*D*).

We further sought to determine the metabolic requirements of the different hypoxic subpopulation of cells by nutrient withdrawal or exposure to specific metabolic inhibitors. Using flow cytometry, we found that glucose and glutamine withdrawal had distinct effects on the 293T-HypoxCR cell subpopulations. In contrast to glutamine deprivation, which resembles control, glucose withdrawal resulted in a significant decrease in the GFP-positive or HIF-positive cells (Fig. S3*A*). We also treated 293T-HypoxCR cells with a glutaminase inhibitor, Bis-2-(5-phenylacetamido-1,2,4-thiadiazol-2-yl)ethyl sulfide (BPTES) (8, 22, 23), and the fatty oxidation inhibitor, etomoxir (24), and found that neither significantly altered the distribution of the hypoxic cell populations (Fig. S3*B*). These observations are consistent with the finding that HIF-positive cells were more glycolytic (Fig. 4*D*) and suggest that the cell subpopulations do not differentially depend on fatty-acid oxidation for survival and are not significantly affected by inhibition of glutamine metabolism. It is notable however, that this behavior may be unique to 293T and, thus, cell type-specific.

The discovery of a distinct subset of hypoxic cells led us to ask whether tumorigenicity is diminished in the non-HIF/noncycling

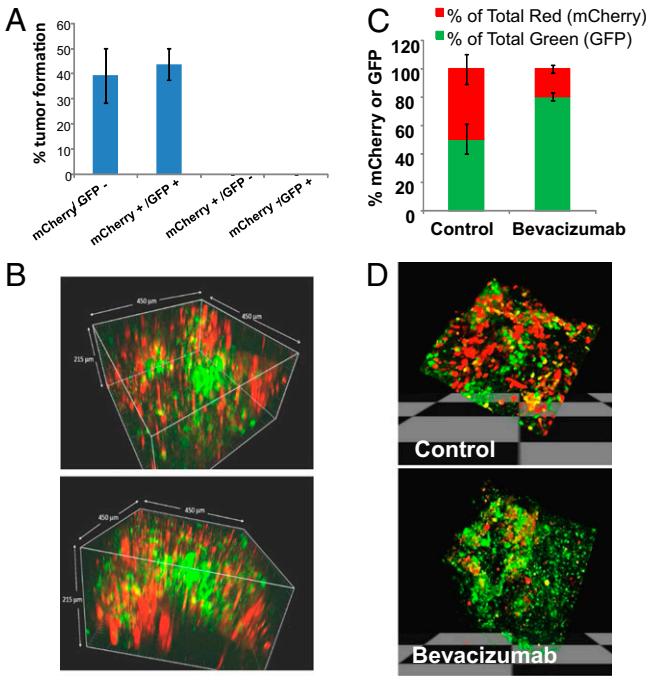

Fig. 5. (*A*) Rates of tumor formation of the 293T-HypoxCR cell subpopulations. Rates of tumor formation are shown as percentages. The experiment was repeated twice, and data are represented as mean ± SEM. (*B*) Confocal microscopy of tumor xenograft. Three-dimensional reconstruction of HEK 293T tumor xenograft images of hypoxic and/or cycling cells marked with the HypoxCR lentiviral reporter. Representative views of a 293T-HypoxCR tumor xenograft reveal subpopulations of tumor cells in vivo. A 215-μm–thick slice of a tumor cut 2 mm from the surface is shown from different angles with a 450 × 450-μm window. Hypoxic (HIF; GFP) cells are green and cycling (mCherry) cells are red; an occasional yellow (HIF/cycling) cell was seen. (*C*) The bar graph shows the percentages of GFP to mCherry cells found in randomly selected tumor areas from replicate experiments with different treatments. Mice bearing tumor xenografts were then either injected with control 5% (vol/vol) DMSO or 100-μg Bevacizumab (Avastin) twice per week. All of the images were randomly selected for five mice of the Control group and seven mice of the Bevacizumab group. The error bars represent SEM. (*D*) Use of HypoxCR to detect therapeutic responses of different tumor subpopulations. Representative 3D confocal micrographs of untreated and treated xenograft tumors are shown.

(non-Warburg) cells compared with those that were HIF-positive. We tested the tumorigenicity of purified subpopulations using a tumor xenograft assay. We injected 10^6 purified cells, which were insufficient for tumor formation, using the original unsorted total population, which required 4×10^6 cells to establish tumors at a rate of 80% over 2 wk after injection. Tumor formation was observed only in HIF/cycling and non-Warburg (non-HIF/noncycling) subgroups (Fig. 5*A*). These observations indicate that a distinct HIF-negative non-Warburg cell population is tumorigenic. However, because of the flexibility of the non-Warburg cell population to replenish other populations (Fig. S2), it is anticipated that this population may have to expand in vivo first into HIF-positive and mCherry-positive (cycling, dividing) cells before going on to form tumors.

Detection of in Vivo Therapeutic Responses by HypoxCR. Currently, in vivo or in situ detection of hypoxia could be achieved through live imaging using positron emission tomography (PET) tracers [^{18}F-fluoromisonidazole (^{18}F-MISO)], oxygen probes for microscopy, injectable fluorescent agents, or immunohistochemistry of fixed tumor tissues (25, 26). In vivo or in situ detection of cell proliferation could be achieved separately through PET imaging using the tracer FLT (18F-labeled nonmetabolized thymidine analog) or Ki-67 staining, respectively (26). The use of HypoxCR, which couples the detection of hypoxia and cell proliferation, further enables the visualization of tumor heterogeneity in situ through two-photon microscopy that yields 3-dimensional reconstructed views (Fig. 5*B*). The images reveal clusters of hypoxic 293T tumor cells (Fig. 5*B*, green) from several angles of the reconstructed 3D image in the center. Cycling cells (Fig. 5*B*, red) are clustered around clusters and cords of hypoxic cells (Fig. 5*B*, green) with occasional hypoxic and cycling cells seen (Fig. 5*B*, yellow).

With HypoxCR, we determined whether this reporter could detect different responses of subpopulations of tumor cells to specific types of therapy. We used bevacizumab (Avastin), an antibody that recognizes and blocks vascular endothelial growth factor A (VEGF-A) (27), to determine whether it affects different subpopulations found in HEK293T tumor xenografts (6). We established tumors with a size of 300 mm^3 and then treated one group ($n = 5$) of animals with control DMSO and another ($n = 7$) with 100 μg of bevacizumab intraperitoneally twice per week. Using in situ imaging with multiphoton confocal microscopy of the treated tumor xenografts, we found that bevacizumab-treated tumors have a significant relative increase in hypoxic cells compared with the controls (P value = 0.04) (Fig. 5 *C* and *D*). This observation is consistent with vascular pruning caused by inhibiting VEGF signaling. Therefore, not only is the HypoxCR reporter a valuable tool to study the tumor microenvironment, but it is also able to indicate which specific tumor-cell subpopulations are sensitive to certain types of drugs.

Conclusion

Our studies demonstrate that HypoxCR can detect a non-Warburg cell population among a mixture of hypoxic cancer cells. These non-Warburg cells are tumorigenic as were ones that were cycling and displayed the Warburg effect, illustrating that complex, varied hypoxic tumor metabolic phenotypes contribute to tumorigenesis. However, because HypoxCR could not be used to track individual cells, we cannot draw conclusions regarding the dynamic relationship between the different cell populations. Nonetheless, the use of HypoxCR illustrates tumor heterogeneity in situ and allows a means to detect the effects of drugs on tumor-cell subpopulations. Along with previous in vivo studies that documented the importance of respiration for RAS-mediated tumorigenesis, our findings offer a cautionary note that therapeutic strategies targeting cancer metabolism should consider the metabolic heterogeneity among hypoxic cancer cells, particularly the non-Warburg respiring cells (28–30).

Materials and Methods

Construction and Characterization of HypoxCR. The lentiviral HypoxCR vector was constructed by standard PCR and subcloning methods and comprises two expression cassettes flanking a spacer sequence, with 2xHRE sites driving a destabilized GFP on one side and a CMV promoter driving a FLAG-tagged fusion gene of mCherry and a codon-optimized version of geminin on the other (see details in *SI Text*).

Purification of HypoxCR-Expressing HEK293T Cells. HEK293T cells were infected with the HypoxCR lentiviral vector and selected with puromycin. Puromycin-selected cells were further purified by flow sorting (see details in *SI Text*).

Metabolic Characterization. Clarke's oxygen electrode was used as described (8). The Seahorse instrument was used according to the manufacturer's instructions.

Imaging of Cellular Heterogeneity in Xenografts of HypoxCR-Expressing HEK293T Cells. Xenografts were explanted, cut at 2mm from the skin surface, and mounted with Vetbond glue to a small Petri dish. The tumor was bathed in saline and imaged in situ with a Zeiss LSM510META confocal with a Coherent Chameleon two-photon laser tuned to 750 nm for mCherry and 910 nm for GFP (see details in *SI Text*).

Animal Studies. Animal study protocols were approved by The Johns Hopkins University Animal Care and Use Committee.

ACKNOWLEDGMENTS. We thank L. Blosser and A. Tam for expertise in flow cytometry and C. Conover Talbot, Jr., for excellent bioinformatics data analysis assistance. Special thanks to the Ross Confocal Microscopy Facility at The Johns Hopkins University School of Medicine. This work was supported by Sol Goldman Pancreatic Cancer Research Fund Grant 80028595; Lustgarten Fund Grant 90049125; Grants NIHR21CA169757 (to A.L.), NIHF32CA174148 (to Z.E.S.), NIH5R01CA051497, and NIH5R01CA057341; Leukemia Lymphoma Society Grant LLS-6363-11; and a Stand-Up-to-Cancer/American Association for Cancer Research translational grant (to C.V.D.). The Seahorse XFe96 Extracellular Flux Analyzer was supported by Award S10RR26474 from the National Center for Research Resources.

1. Dang CV (2012) Links between metabolism and cancer. *Genes Dev* 26(9):877–890.
2. Vander Heiden MG, Cantley LC, Thompson CB (2009) Understanding the Warburg effect: The metabolic requirements of cell proliferation. *Science* 324(5930):1029–1033.
3. Cairns RA, Harris IS, Mak TW (2011) Regulation of cancer cell metabolism. *Nat Rev Cancer* 11(2):85–95.
4. Keith B, Johnson RS, Simon MC (2012) HIF1α and HIF2α: Sibling rivalry in hypoxic tumour growth and progression. *Nat Rev Cancer* 12(1):9–22.
5. Semenza GL (2012) Hypoxia-inducible factors: Mediators of cancer progression and targets for cancer therapy. *Trends Pharmacol Sci* 33(4):207–214.
6. Koppenol WH, Bounds PL, Dang CV (2011) Otto Warburg's contributions to current concepts of cancer metabolism. *Nat Rev Cancer* 11(5):325–337.
7. Fogal V, et al. (2010) Mitochondrial p32 protein is a critical regulator of tumor metabolism via maintenance of oxidative phosphorylation. *Mol Cell Biol* 30(6): 1303–1318.
8. Le A, et al. (2012) Glucose-independent glutamine metabolism via TCA cycling for proliferation and survival in B cells. *Cell Metab* 15(1):110–121.
9. Sonveaux P, et al. (2008) Targeting lactate-fueled respiration selectively kills hypoxic tumor cells in mice. *J Clin Invest* 118(12):3930–3942.
10. Chandel NS, Budinger GR, Choe SH, Schumacker PT (1997) Cellular respiration during hypoxia: Role of cytochrome oxidase as the oxygen sensor in hepatocytes. *J Biol Chem* 272(30):18808–18816.
11. Raman V, et al. (2006) Characterizing vascular parameters in hypoxic regions: A combined magnetic resonance and optical imaging study of a human prostate cancer model. *Cancer Res* 66(20):9929–9936.
12. Dewhirst MW, Cao Y, Moeller B (2008) Cycling hypoxia and free radicals regulate angiogenesis and radiotherapy response. *Nat Rev Cancer* 8(6):425–437.
13. Kimura H, et al. (1996) Fluctuations in red cell flux in tumor microvessels can lead to transient hypoxia and reoxygenation in tumor parenchyma. *Cancer Res* 56(23): 5522–5528.
14. Sakaue-Sawano A, et al. (2008) Visualizing spatiotemporal dynamics of multicellular cell-cycle progression. *Cell* 132(3):487–498.
15. Gardner LB, et al. (2001) Hypoxia inhibits G1/S transition through regulation of p27 expression. *J Biol Chem* 276(11):7919–7926.
16. Green SL, Freiberg RA, Giaccia AJ (2001) p21(Cip1) and p27(Kip1) regulate cell cycle reentry after hypoxic stress but are not necessary for hypoxia-induced arrest. *Mol Cell Biol* 21(4):1196–1206.
17. Hubbi ME, et al. (2013) A nontranscriptional role for HIF-1α as a direct inhibitor of DNA replication. *Sci Signal* 6(262):ra10.
18. Hu CJ, Sataur A, Wang L, Chen H, Simon MC (2007) The N-terminal transactivation domain confers target gene specificity of hypoxia-inducible factors HIF-1alpha and HIF-2alpha. *Mol Biol Cell* 18(11):4528–4542.
19. Eisen MB, Spellman PT, Brown PO, Botstein D (1998) Cluster analysis and display of genome-wide expression patterns. *Proc Natl Acad Sci USA* 95(25):14863–14868.
20. Subramanian A, et al. (2005) Gene set enrichment analysis: A knowledge-based approach for interpreting genome-wide expression profiles. *Proc Natl Acad Sci USA* 102(43):15545–15550.
21. Liu YC, et al. (2008) Global regulation of nucleotide biosynthetic genes by c-Myc. *PLoS ONE* 3(7):e2722.
22. Seltzer MJ, et al. (2010) Inhibition of glutaminase preferentially slows growth of glioma cells with mutant IDH1. *Cancer Res* 70(22):8981–8987.
23. DeLaBarre B, et al. (2011) Full-length human glutaminase in complex with an allosteric inhibitor. *Biochemistry* 50(50):10764–10770.
24. Zhang J, et al. (2012) Measuring energy metabolism in cultured cells, including human pluripotent stem cells and differentiated cells. *Nat Protoc* 7(6):1068–1085.
25. Arteel GE, Thurman RG, Yates JM, Raleigh JA (1995) Evidence that hypoxia markers detect oxygen gradients in liver: Pimonidazole and retrograde perfusion of rat liver. *Br J Cancer* 72(4):889–895.
26. Farwell MD, Pryma DA, Mankoff DA (2014) PET/CT imaging in cancer: Current applications and future directions. *Cancer*, 10.1002/cncr.28860.
27. Weisshardt P, et al. (2012) Tumor vessel stabilization and remodeling by anti-angiogenic therapy with bevacizumab. *Histochem Cell Biol* 137(3):391–401.
28. Weinberg F, et al. (2010) Mitochondrial metabolism and ROS generation are essential for Kras-mediated tumorigenicity. *Proc Natl Acad Sci USA* 107(19):8788–8793.
29. Guo JY, et al. (2011) Activated Ras requires autophagy to maintain oxidative metabolism and tumorigenesis. *Genes Dev* 25(5):460–470.
30. Son J, et al. (2013) Glutamine supports pancreatic cancer growth through a KRAS-regulated metabolic pathway. *Nature* 496(7443):101–105.